Temporal variation of ^{129}I and ^{127}I in aerosols from Xi'an, China: influence of East Asian monsoon and heavy haze events

Luyuan Zhang [1,2,5*], Xiaolin Hou [1,2,3,5], Sheng Xu [4], Tian Feng [1], Peng Cheng [1], Yunchong Fu [1], Ning Chen [1]

[1]State Key Laboratory of Loess and Quaternary Geology, Shaanxi Key Laboratory of Accelerator Mass Spectrometry Technology and Application, Xi'an AMS Center, Institute of Earth Environment CAS, Xi'an 710061, China

[2]Center for Excellence in Quaternary Science and Global Change, Chinese Academy of Sciences, Xian 710061, China

[3]Center for Nuclear Technologies, Technical University of Denmark, Risø Campus, Roskilde 4000, Denmark

[4]Institute of Surface-Earth System Science, Tianjin University, Tianjin 300072, China

[5]Open Studio for Oceanic-Continental Climate and Environment Changes, Pilot National Laboratory for Marine Science and Technology (Qingdao), Qingdao 266061, China

Correspondence to: Luyuan Zhang (zhangluyuan.118@163.com; zhangly@ieecas.cn)

Abstract. Aerosol iodine isotopes are pivotal links in atmospheric circulation of iodine in both atmospheric and nuclear sciences, while their sources, temporal change and transport mechanism are still not well understood. This work presents the day-resolution temporal variation of iodine-129 (^{129}I) and iodine-127 (^{127}I) concentrations in aerosols from Xi'an, northwest China during 2017/2018. Both iodine isotopes have significant fluctuations with time, showing highest levels in winter, approximately two to three times higher than in other seasons, but the correlation between ^{129}I and ^{127}I concentrations reflects they have different sources. Aerosol ^{127}I concentrations are found to be noticeably positively correlated with air quality index and five air pollutants. Enhanced fossil fuel combustion and inverse weather conditions can explain the increased concentrations and peaks of ^{127}I in winter. The change of ^{129}I concentrations confirms that source and level of ^{129}I in the monsoonal region were alternatively dominated by the ^{129}I-enriched East Asian winter monsoon and the ^{129}I-poor East Asian summer monsoon. The mean $^{129}I/^{127}I$ number ratio of (92.7±124) $\times 10^{-10}$ provides an atmospheric background level for the purpose of nuclear environmental safety monitoring. This study suggests that locally discharged stable ^{127}I and externally input ^{129}I are likely involved into fine particles formation in urban air, shedding insights into long-range transport of air pollutants and iodine's role in particulate formation in urban atmosphere.

1 Introduction

Iodine is one of active halogen elements, and involved into plenty of atmospheric chemical reactions (i.e. ozone depletion and new particles formation from condensable iodine-containing vapours), drawing increasing attention in not only atmospheric science, but also environmental fields in recent years (Saiz-Lopez et al., 2012). A number of studies on atmospheric iodine just focus on the processes and mechanisms in marine boundary layer since over 99.8% of iodine derives from ocean

(McFiggans et al., 2000). Other sources of iodine in air comprise volatile iodine and resuspended particles from soil, as well as combustion of fossil fuel (Fuge and Johnson, 1986). Whitehead et al. (1984) estimated annual release of iodine from fossil fuel combustion is about 400 tons, accounting for only 0.1% of total iodine in air. In contrast, anthropogenic iodine in Chinese megacities is believed to be significantly underestimated due to coal combustion (Wu et al., 2014). A few studies have shown high iodine concentrations in air and particles in China (Gao et al., 2010; Xu et al., 2010). Although marine atmospheric iodine has been proven to form fine particles, little is known about terrestrial atmospheric iodine, particularly in urban sites with severe air pollution.

Along with atmospheric circulation of stable ^{127}I, long-lived radioactive ^{129}I with half-life of 15.7 million years is also of importance in global transport since it is a major fission product with a yield of 0.7% in nuclear industry. China is in transition phase of energy structure to solve environmental pollution issues, and has put great emphasis on developing nuclear power (World Nuclear Association, 2017). Nuclear waste reprocessing is also in the process of construction in China, which may be a key source of ^{129}I in the future. Investigation on level, sources, temporal changes are extremely necessary for nuclear environmental safety assessment and nuclear emergency preparedness. Environmental $^{129}I/^{127}I$ number ratios have been increased from natural ^{129}I level of 10^{-12} to anthropogenic level beyond 10^{-10} in modern environment due to the atmospheric nuclear weapon testing, nuclear accidents, nuclear fuel reprocessing process, etc (Snyder et al., 2010). More than 95% of the environmental ^{129}I was discharged by the two European nuclear fuel reprocessing plants (NFRPs), Sellafield in United Kingdom and La Hague in France to the seas and air in liquid and gaseous forms, respectively. As a consequence of ^{129}I releases from NFRPs, nuclear accidents and nuclear weapon testing sites, the global distribution of ^{129}I is rather uneven (Snyder et al., 2010). Atmospheric ^{129}I investigations have been conducted in Europe, Japan, USA and Canada, but aerosol ^{129}I studies are still rare, and no aerosol ^{129}I data is available in China at present (Hasegawa et al., 2017; Hou et al., 2009; Jabbar et al., 2013; Moran et al., 1999; Toyama et al., 2013; Xu et al., 2013). Furthermore, those previous studies present time series of ^{129}I in aerosols in monthly resolution for the purpose of nuclear environmental monitoring. Such a low time-resolution is not sufficient to understand the sources, transport and temporal variation pattern and its influencing factor of ^{129}I.

Here, we present a day-resolution temporal variation of ^{129}I and ^{127}I in aerosols during 2017/2018 from a typical monsoonal zone, Xi'an city in the Guanzhong Basin of northwest China, to make attempts to investigate the level, sources and temporal change characteristics of ^{127}I and ^{129}I. This study will help to establish a background value of $^{129}I/^{127}I$ number ratio serving the nuclear environmental safety monitoring. The possible influencing factors on temporal variation of iodine isotopes are also explored, including meteorological parameters, East Asian monsoon (EAM) and heavy haze events.

2 Materials and methods

The aerosol samples were collected using a high-volume sampler on the roof of Xi'an AMS Center (34°13'25"N, 109°0'0"E) with an elevation of 440 m above mean sea level (Fig. 1). Xi'an, located in the Guanzhong basin, is the largest city in northwest

China with a population of 9.9 million. The basin is nestled between Qinling mountains in the south and the Loess Plateau in the north, and is warm temperate zone with semi-humid continental monsoon climate (Fig. 1b).

Sixty-eight aerosol samples were selected for measurement of iodine isotopes using the pyrolysis combined with AgI-AgCl coprecipitation for separation. The sample collection and preparation procedure are described in detail in the supplementary information (SI-1), as previously reported (Zhang et al., 2018b). Accelerator mass spectrometry (AMS, 3MV, HVEE, the Netherland) and inductively coupled plasma mass spectrometry (ICP-MS, Agilent 8800, USA) were applied for determination of $^{129}I/^{127}I$ number ratios and ^{127}I concentrations, respectively. $^{129}I/^{127}I$ number ratio of iodine carrier is less than 2×10^{-13}, and the analytical precisions are within 5% for all the aerosol samples.

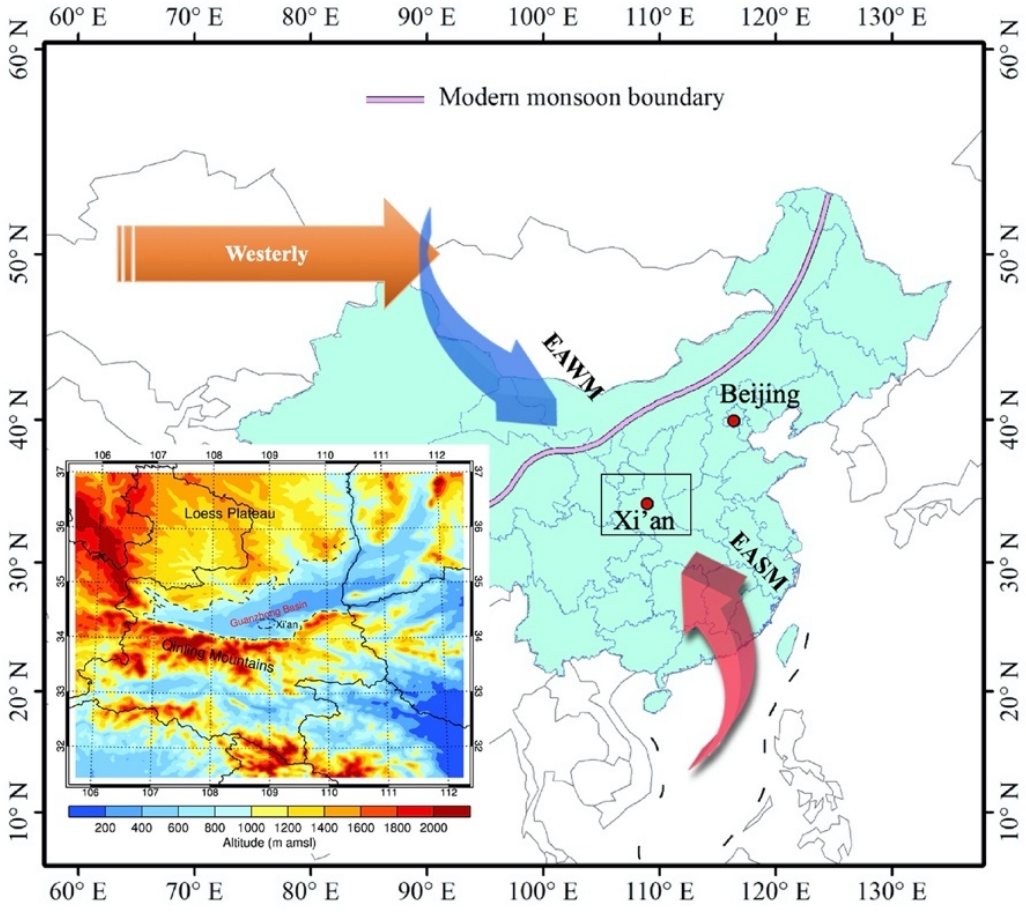

Fig. 1 Map showing the sampling location (Xi'an city in rectangle) and East Asian monsoon (EAM) system. The inset shows the topography of the studied area in the Guanzhong Basin between the Loess Plateau to the north and Qinling Mountains to the south. East Asian monsoon, constituted by East Asian summer monsoon (EASM) and East Asian winter monsoon (EAWM), is one of vital components of the global atmospheric circulation system. The pink line in the map is the modern monsoon boundary, and the arrows indicate the westerly (orange), the EAWM (blue) and the EASM (red).

3 Results

Results of ^{127}I concentrations ($\gamma(^{127}I)$) and ^{129}I concentrations ($N(^{129}I)$), $^{129}I/^{127}I$ number ratios in aerosol samples in Xi'an, China from March 2017 to March 2018, are shown in Fig. 2. Concentrations of ^{127}I and ^{129}I and $^{129}I/^{127}I$ number ratios fell within 1.21-21.4 ng m^{-3}, (0.13-7.53) $\times 10^5$ atoms m^{-3}, and (10.6-743) $\times 10^{-10}$, respectively. The mean values were 6.22±4.48 ng m^{-3}, (1.97±1.65) $\times 10^5$ atoms m^{-3}, and (92.7±124) $\times 10^{-10}$ for $\gamma(^{127}I)$, $N(^{129}I)$ and $^{129}I/^{127}I$ number ratios, respectively.

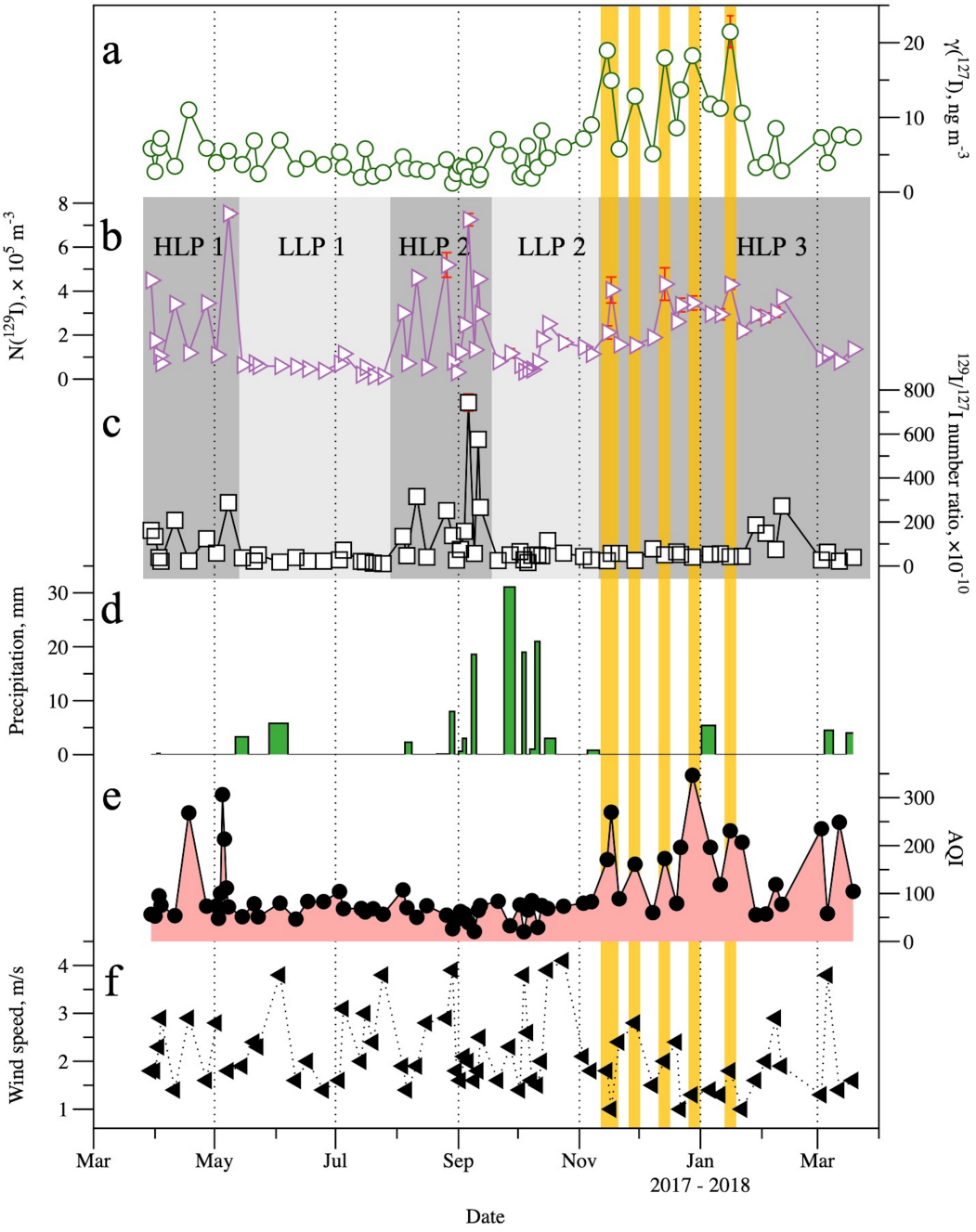

Fig. 2 Temporal variation of ^{127}I (a), ^{129}I (b) and ^{129}I/^{127}I number ratios (c) in aerosol samples collected in Xi'an, China from March 2017 to March 2018. The meteorological and air quality data includes precipitation (d), Air quality index (AQI, e) and wind speed (f). Orange bands indicate five heavy haze episodes corresponding with five ^{127}I peaks. Three dark and two light grey shades in b and c demonstrate the high-level and low-level periods (HLP and LLP), respectively, for ^{129}I and ^{129}I/^{127}I number ratios, alternatively dominated by the EAWM and EASM, respectively.

^{127}I and ^{129}I in aerosols are characterized with apparently monthly and seasonal variations (Fig. 3 and 4). The minimum and maximum of monthly concentrations were observed in August and December for ^{127}I, and July and December for ^{129}I, respectively. The average $\gamma(^{127}I)$ in November, December and January (11.4-12.7 ng m^{-3}) were two times higher than in other months (3.12-6.70 ng m^{-3}). Distinct from ^{127}I, monthly variation of ^{129}I shows the lowest level in June and July ((0.47-0.50) $\times 10^5$ atoms m^{-3}), about two to six times lower than the other months. The maximum of $^{129}I/^{127}I$ number ratio was not observed in winter months but in September.

The average $\gamma(^{127}I)$ were 5.68±2.24 ng m^{-3}, 3.61±1.49 ng m^{-3}, 6.05±4.52 ng m^{-3}, and 10.6±6.0 ng m^{-3} in spring, summer, fall and winter, respectively. The level of ^{127}I in winter was about two times higher than spring and fall, three times higher than summer. $N(^{129}I)$ were (1.93±1.90) $\times 10^5$ atoms m^{-3}, (1.17±1.55) $\times 10^5$ atoms m^{-3}, (1.92±1.62) $\times 10^5$ atoms m^{-3}, and (3.12±0.72) $\times 10^5$ atoms m^{-3} in spring, summer, fall and winter, respectively. The level of ^{129}I in winter was about two times higher than spring and fall, and 3.3 times higher than summer. Seasonal variation of $^{129}I/^{127}I$ number ratios was not such obvious as the concentrations of iodine isotopes. The mean $^{129}I/^{127}I$ number ratio of (119±185) $\times 10^{-10}$ in fall were slightly higher than those of (82.2±79.3) $\times 10^{-10}$ in spring, (71.5±89.3) $\times 10^{-10}$ in summer and (89.3±70.5) $\times 10^{-10}$ in winter. Whereas, the ratios in all four seasons fell in the similar range as that of the whole year.

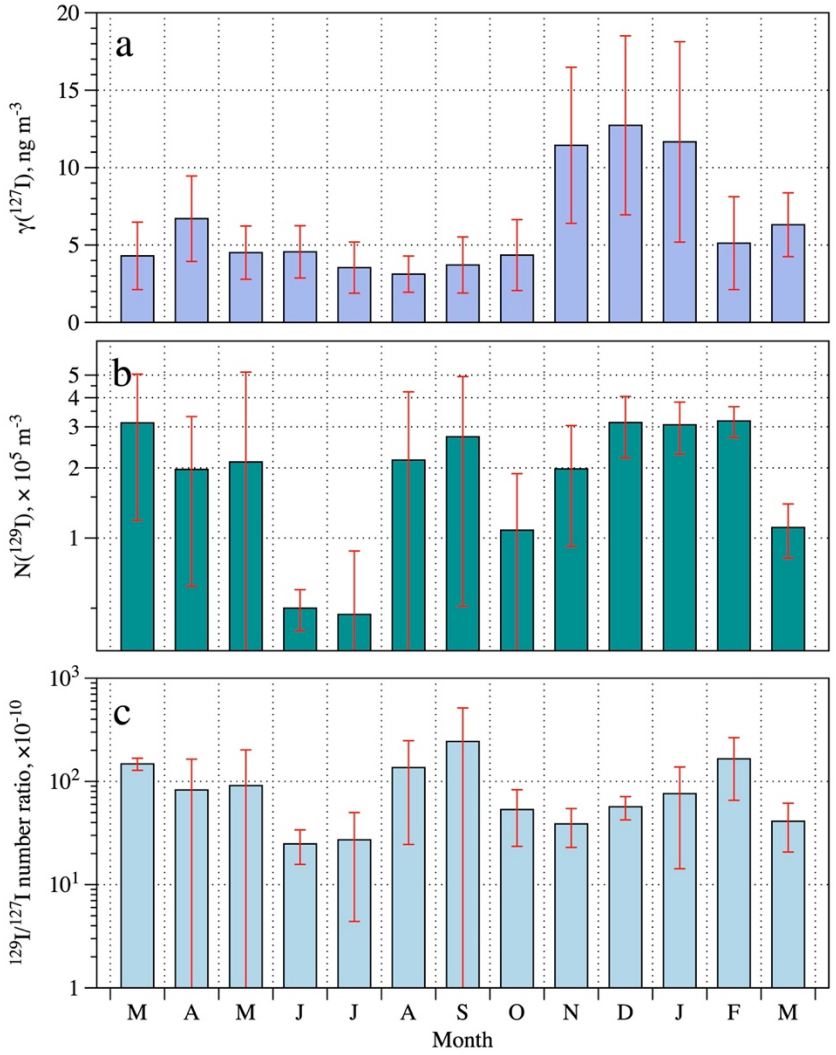

Fig. 3 Monthly variation of ^{127}I (a), ^{129}I (b) and $^{129}I/^{127}I$ number ratios (c) in aerosols from March 2017 to March 2018.

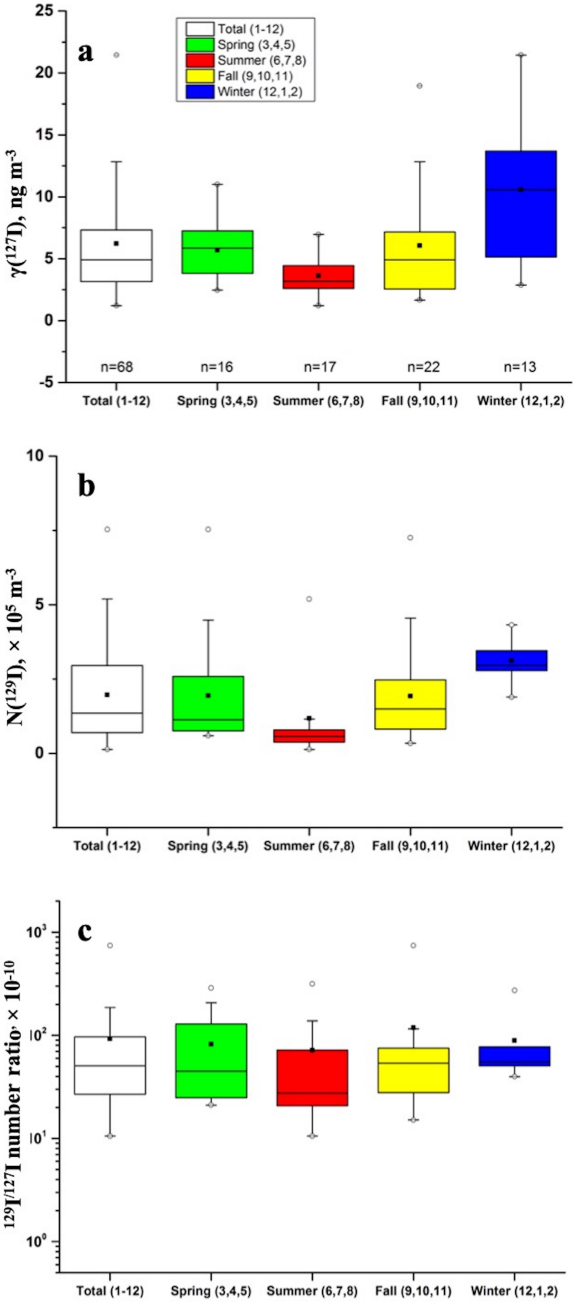

105

Fig. 4 Seasonal variation of ^{127}I (a), ^{129}I (b) and $^{129}I/^{127}I$ number ratios (c) in aerosols collected in Xi'an, China from March 2017 to March 2018. The boxes show the range from 25% to 75%. Mean and median values are indicated with black solid squares and horizontal bars, respectively. The whisker indicates the upper and lower limits excluding outliers shown by dots. The outliers are defined as those 1.5 times greater than the interquartile range.

110

A weak correlation between ^{129}I and ^{127}I was found with Spearman correlation coefficient of 0.33 ($p<0.01$) for the whole year data, while no significant correlation between the two iodine isotopes in each season at the level of 0.05 (Table 1 and Fig. S1). The correlation analysis between iodine isotopes and total suspended particle (TSP) indicate that there was a strong correlation between ^{127}I and TSP, while no correlation between radioactive ^{129}I and TSP (Fig. S2).

4 Discussion

4.1 Level and sources of ^{127}I and ^{129}I

The results of a weak correlation in the whole year sampling and no significant correlations in each season between the two isotopes indicate that ^{127}I and ^{129}I have different sources and influence factors.

4.1.1 ^{127}I

The level of ^{127}I concentrations, in particular in winter, is much higher than those in continental sites (below 0.61 ng m^{-3} in South Pole and 2.7-3.3 ng m^{-3} in the Eastern Transvaal), and comparable to those in coastal and ocean sites (typically below 20 ng m^{-3}, and up to 24 ng m^{-3} in tropic marine aerosols) (Saiz-Lopez et al., 2012). A similar range of ^{127}I in TSP was observed to be 4.5-22 ng m^{-3} at a coastal urban, Shanghai, China, showing lowest in summer and an increase occurred in fall and winter (Gao et al., 2010). Iodine associated with PM10 and PM2.5 were found to be 3.0-115 ng m^{-3} and 4-18 ng m^{-3}, respectively, in urban and island sites of Shanghai, slightly lower than TSP iodine (Cheng et al., 2017; Gao et al., 2010). The marine aerosol iodine offshore China was found below 8.6 ng m^{-3} during the XueLong cruise from July to September 2008 (Xu et al., 2010). The results suggest a relatively high aerosol ^{127}I level in both inland and coastal urbans in China.

Natural iodine in air is from marine emission through sea spray and gaseous emissions from seas, weathering of base rock and continental release through vegetation and suspended soil particles (Carpenter et al., 2013; Fuge and Johnson, 1986). Due to the influence of southeasterly EASM, moisture from the Pacific Ocean and the Chinese seas might bring marine iodine. Whereas, the mean $\gamma(^{127}I)$ in summer aerosol is 3.61±1.49 ng m^{-3}, about three-fold lower than that in winter. The sampling location, Xi'an, is an inland city about 900 km away from the nearest coastline. The contribution of marine iodine to terrestrial surface system in winter is considered to be negligible when the site is over 400 km away from the ocean (Cohen, 1985). Taking sodium and calcium as reference elements for sea spray and direct volatilization of iodine from the ocean and weathering of soil and rock, respectively, He et al. (2012) has been estimated that less than 0.04% and 5.2% of iodine were from direct marine contribution and weathering of soil and rock, respectively, to the precipitation at Zhouzhi county, Xi'an city (He, 2012). Despite being likely underestimated, marine iodine contribution in precipitation samples showed a decline trend with increasing distance of 20 km to 1252 km from the sea. And no significant change of marine contribution could be found over 100 km from the sea (He, 2012).

Iodine is also emitted from volatility of terrestrial soil and respiration of vegetation, which was estimated to be 2.27 μg m^{-2} d^{-1} in the form of CH_3I, on a global basis, over an active season of 240 days, together with biome areas for temperate forest and

wood lands (28.5×10^{12} m^2) and temperate grasslands (31.9×10^{12} m^2) (Sive et al., 2007). Dry deposition flux of iodine, however, can be calculated to be 5.83-40.7 μg m^{-2} d^{-1} based on aerosol ^{127}I mass concentrations in TSP (13.3-92.5 μg g^{-1} TSP) multiplying an annual average dustfall flux of 13.2 t (km^{-2} 30 d^{-1}) (Xi'an Bureau of Statistics, 2018). The uncertainty for the calculation is about 32% mainly due the large uncertainty of dustfall flux of about 31%. Because of different land coverage between urban and forest-grassland in reference of Sive et al. (2007), terrestrial emission of iodine in the sampling site should be even lower than 2.27 μg m^{-2} d^{-1}. The dry deposition flux of iodine in Xi'an was therefore far beyond terrestrial sources of soil and vegetations, indicating they might be important iodine sources in summer, but not in winter.

The significant increase of ^{127}I from summer to winter suggests that anthropogenic discharge of iodine is the dominant source of ^{127}I in Xi'an aerosol samples, mainly including combustion of biomass and fossil fuel (Wu et al., 2014). Biomass combustion generally occurs in summer harvest time, normally in later May and early June. In order to improve air quality, Xi'an government has banned biomass combustion since 2009. Additionally, no obvious change in ^{127}I concentrations was found in May and June, indicating the biomass combustion is not the major source.

A recent study has confirmed that particulate iodine around two coal plants in Nanchang city, China, was greatly increased up to 36 ng m^{-3}, and iodine concentrations within 9 km from the coal plants were much higher than that in non-coal sites (Duan, 2018). Coal is dominant in energy consumption structure. Coal consumption accounts for 72.7% of total energy consumption in Shaanxi province in 2013. In 2017, the coal consumption in Guanzhong basin is 67.4 million tons (Shaanxi Provincial Bureau of Statistics, 2018). ^{127}I concentration in coal produced in Shaanxi province ranges from 0.39 to 6.53 μg g^{-1} with a mean value of 1.47 μg g^{-1} (Wu et al., 2014). An atmospheric iodine emission factor that equals to the ratio of the iodine released into the atmospheric from the coal is from 78.8% to 99.4%, depending on the coal combustion technology and emission control devices (Wu et al., 2014). If simply assuming anthropogenic iodine is solely from combustion of coal in the study area and the atmospheric iodine emission factor is 92%, about 91 tons of ^{127}I can be released to the atmosphere in the Guanzhong Basin in 2017. Xi'an, a northern city in China, consumes more coals in the heating period from November 15 to March 15, which aggravates iodine release from coal combustion. Thus, we suggest that coal combustion is the major source of ^{127}I in Xi'an urban aerosols in particular during the heating period of winter. This also suggests that ^{127}I was regionally or locally input, and can be treated as internal release.

4.2.2 ^{129}I

The aerosol ^{129}I levels reported in the previous studies and this work could be categorized into three groups (Fig.5). 1) Compared to other investigating sites, aerosol N(^{129}I) were less than 10^6 atoms m^{-3} in Xi'an, northwest China. This low level is also found at those sites remote from the nuclear facilities in southern and central Europe, as well as Japan before the Fukushima accident (Hasegawa et al., 2017; Jabbar et al., 2013; Santos et al., 2005). The lowest N(^{129}I) ($< 0.1 \times 10^5$ atoms m^{-3}) in aerosols have been found at two high altitude sites of Alps mountains (about 3000 m above the sea level). 2) The high values beyond 10^8 atoms m^{-3} have been reported at the sites directly contaminated either by nuclear reprocessing plants, such as Hanford, Sellafield and WAK at Karlsruhe, or by Fukushima nuclear accident in 2011 (Brauer et al., 1973; Jackson et al.,

2002; Wershofen and Aumann, 1989; Xu et al., 2015). 3) In between, aerosol N(^{129}I) within the range from 10^6 atoms m^{-3} to 10^8 atoms m^{-3}, are mainly found in the sites and periods with global fallout from atmospheric nuclear weapon testing, and indirectly contaminations from nuclear fuel reprocessing plants (Brauer et al., 1973; Englund et al., 2010; Kadowaki et al., 2018; Tsukada et al., 1991; Zhang et al., 2016).

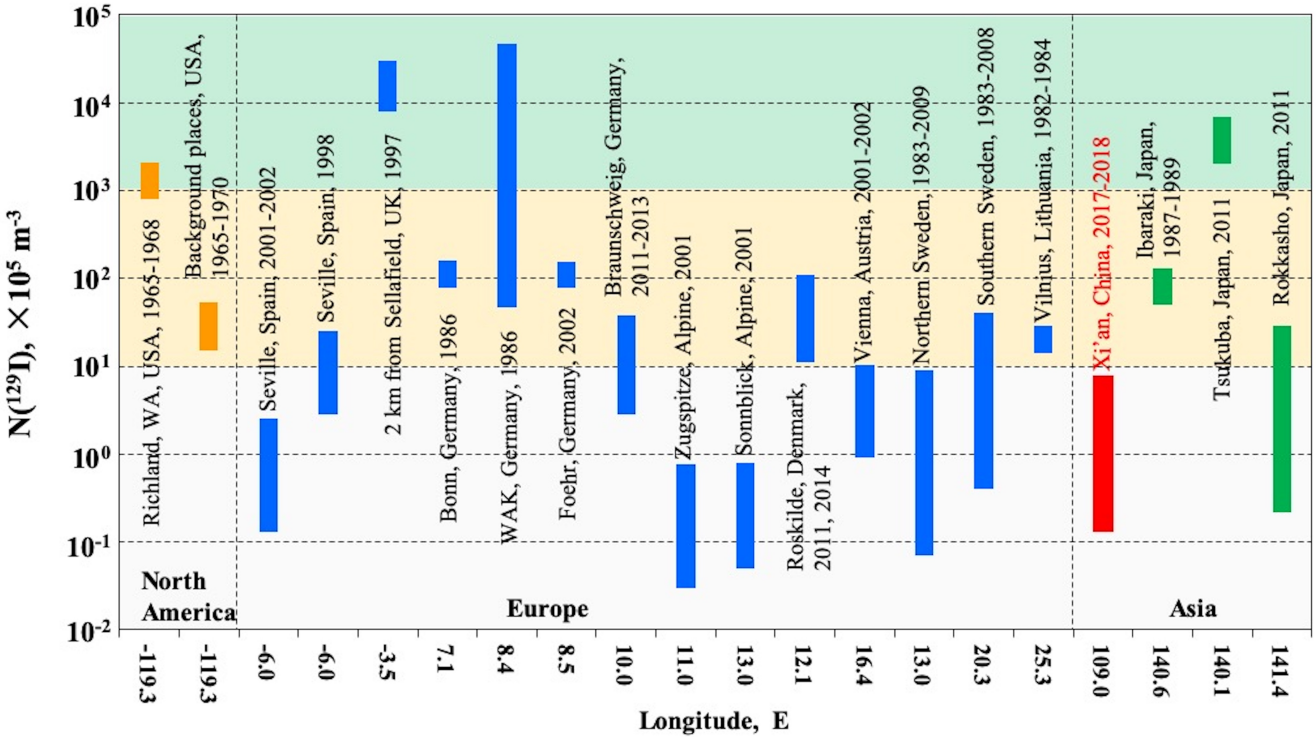

Fig. 5 Comparison of aerosol ^{129}I levels in Xi'an, China (red bars) with other investigations in North America (orange), Europe (blue) and East Asia (Green) distributed by longitude. The green, yellow and white bands are high (> 10^8 atoms/m^3), middle (10^6 to 10^8 atoms/m^3) and low (< 10^6 atoms/m^3) ^{129}I concentrations in aerosols.

The source term of ^{129}I is crucial for spatial and temporal distributions of ^{129}I in global scale. ^{129}I/^{127}I number ratios in the Xi'an aerosols range from 10.6×10^{-10} to 743×10^{-10}, at least three orders of magnitude higher than naturally produced ^{129}I level (1.5×10^{-12}) (Fehn et al., 2005). This clearly indicates human nuclear activities are dominant contributor for the increase of ^{129}I level in the environment. The level and source of ^{129}I in soil, vegetation, rain and rivers water samples have been previously investigated in Xi'an region, where ^{129}I/^{127}I varied from 1.1×10^{-10} to 43.5×10^{-10} with a mean value of 20.6×10^{-10} (Zhang et al., 2011). Aerosol ^{129}I/^{127}I number ratios were about one order of magnitude higher than those in other environmental media, indicating ^{129}I in Xi'an aerosols was not released by local soil suspension and vegetation release. Weathering of bed rock is neither a major source of airborne ^{129}I, since weathering just contributes 5% of stable iodine, and ^{129}I in bed rock can be

considered even lower than the nature-produced ^{129}I level because of the continuous decay. Coal combustion contributes a large proportion of stable ^{127}I in winter, while ^{129}I amount in coals is almost negligible, because coal was formed in Tertiary (2.58-66 million years) at the latest so that ^{129}I has been decayed out or in an extremely low value of 10^{-13}~10^{-10} for $^{129}I/^{127}I$. Thus, coal combustion is not a major source of atmospheric ^{129}I.

Nuclear activities including the historic nuclear weapon testing sites, nuclear reactors, NFRPs in China and Europe, as well as the underground nuclear weapon testing are considered. Two nuclear weapon testing sites, Semipalatinsk and Lop Nor, locating upwind, may input ^{129}I into Xi'an region through soil resuspension and gaseous re-emission. However, evidence from ^{129}I distribution in surface soils from upwind regions reveals that the two nuclear weapon testing sites has limit impact on the atmospheric ^{129}I level in the remote regions farther than 1000 km from these test sites (Fan, 2013). This is also supported by the back-trajectory analysis that ^{129}I concentration did not significantly raised when abundant air masses from Xinjiang passing through the Lop Nor test site on December 28, 2018 (Fig. S3g). Five nuclear power plants are in operation along the southeast coastal areas in China. ^{129}I data in sea water collected within 10 km from a Chinese nuclear power plant suggests that normal operation of reactors does not have significant increase in ^{129}I concentrations (He et al., 2011). Although information on gaseous release of ^{129}I from these reactors is unknown, the low $^{129}I/^{127}I$ (about 7×10^{-10}) in the surface soil of southern China (Guangxi, Jiangxi and Fujian Provinces) close to the reactors can confirm that there is no marked deposition from the gaseous release (Fan, 2013). Toyama et al. (2013) have shown a direct close-in influence of a pilot plant in Tokaimura (Ibaraki Prefecture), Japan on the ^{129}I deposition in Tokyo. Similarly, a pilot nuclear spent fuel reprocessing plant (NFRP) has been established and operated in Gansu province, China since 2010. This NFRP is locating in an upwind area and about 1200 km northeast of Xi'an. During the sampling period in 2017/2018, no abnormally high ^{129}I was observed, while this contribution cannot be neglected in the future operation, and should be continuously monitored. In addition, the possible influence of the sixth underground nuclear weapon test conducted by North Korea on September 3, 2017 has been excluded based on the back and forward trajectories and the nuclear environmental monitoring around the Chinese northeast border by the government (Ministry of Environmental Protection of the People's Republic of China, 2017).

It is well documented that gaseous and liquid discharges from the NFRPs in Sellafield, United Kingdom and La Hague, France, as well as the secondary emission from the contaminated seas and land, are the predominant source of ^{129}I in the modern atmosphere, in particular in European environment (Jabbar et al., 2013). The two NFRPs are located in the 50-55°N, the westerly belt. The prevailing westerly winds throughout the year in the mid-latitude act as a crucial pathway of ^{129}I transport from its source to the whole mid-latitude regions of the northern hemisphere, as observed in the sediment core from Jiaozhou Bay, east coast of China (Fan et al., 2016). The 60-year record of ^{129}I in a lacustrine sediment from Philippines further shows that the EAWM plays an important role in transporting the mid-latitude ^{129}I to the low-latitude regions (Zhang et al., 2018a). The feature of ^{129}I variation also shows that ^{129}I was in high level in spring and winter when EAWM prevailing and low level in summer when EASM prevailing, supporting that the ^{129}I is dominantly sourced from the long-range transport of European NFRPs discharges. In this case, ^{129}I is externally input in contrast to the locally released stable ^{127}I.

4.2 Factors influencing temporal variation of iodine isotopes

As discussed above, even though variation pattern of ^{127}I and ^{129}I were similar, they were considerately influenced by many factors owing to their different sources. In this work, meteorological factors including precipitation, wind speed, temperature and dust storm events, atmospheric circulation (in particular EAM), heavy air pollution periods are discussed.

4.2.1 Meteorological factors

Precipitation and wind speed. As discussed in supplementary information (SI-2), the influences of precipitation and wind speed on temporal changes of iodine isotopes are not significant (Fig. 2e and 2f). However, the winter days with absence of wet precipitation and lower wind speed well corresponded to the heavy haze episodes when iodine concentrations, in particular stable ^{127}I, were greatly increased, indicative of less dispersion. The details about haze influence on iodine will also be discussed in the following section.

Temperature. Temperature and its associated physiochemical processes and biological release of iodine from source regions might be reasons for the variation patterns. In summer, the temperature is about 20-40°C in North hemisphere, which is favourable for direct volatilization of iodine from the surfaces of land and seas. Ozone in air-sea boundary layer is suggested to act as an oxidants to transform iodide in seawater to volatile molecular iodine that enters into the air, which is believed more significant than the biological process (Carpenter et al., 2013). Ozone concentrations in summer is around 30 nmol mol^{-1}, roughly two times higher than winter (Ayers et al., 1996), which may increase re-emission rate of iodine from the ocean and ^{129}I-contaminated sea surface into the air. Additionally, the bloom of phytoplankton and algae in summer, can release biogenic organic iodine into the air through a mechanism of anti-oxidation (Küpper et al., 2008). The temperature, ozone concentration and marine biomass greatly reduces in winter, which will result in less iodine released from the source regions, and can be used to explain the relatively weak peaks in winter than in summer. As discussed above, ^{127}I and ^{129}I in Xi'an aerosols were mainly derived from coal combustion and long-range transport from Europe, respectively. The change in release amount of ^{127}I and ^{129}I at the source regions is obviously not the determining factor for the changes of iodine isotopes since Xi'an is far from the oceans and the ^{129}I source regions. Furthermore, the seasonal variation of ^{127}I and ^{129}I with low level in summer can also easily exclude the possibility of temperature influence.

In addition to atmospheric stability reflected by precipitation, wind and temperature, atmospheric boundary layer height determines vertical dispersion scale of air pollutions by thermal turbulent mixing, which might be a factor for variation of iodine isotopes. Since ^{127}I is locally input and ^{129}I is remotely transported from Europe, the influence of boundary layer height might be different for the two iodine isotopes. It will be further explored with longer temporal variation of iodine isotopes in the future.

Dust storm. Two severe dust storm events occurred in Xi'an in 17-18 April and 4-6 May, 2017, as indicated by the peaks of air quality index (AQI) of 268 and 306, respectively. A ^{127}I peak, 11.0 ng m^{-3}, was observed on 18 April, 2017, while ^{127}I levels in other samples were almost below 6 ng m^{-3} in spring and summer time. Dust storms frequently occur in winter and

spring in north China, and normally originate from the arid and semi-arid desert regions mainly locating in Mongolia and northwest China. The first dust storm arrived the Guanzhong basin on 17 April 2017, and lasted until 19 April (China Meteororological Administration, 2017). The small peak of ^{127}I is likely attributed to the suspended particulate matter from the soil surface in the dust storm source. In contrast, variation of ^{129}I level did not reflect the dust storm influence. The fact that ^{129}I was not correlated with particulate concentrations (Fig. S4), indicates that the extrinsic ^{129}I is not related to the heavy particulate events, since the major dust source areas include Taklimakan desert, the Gobi Desert in Inner Mongolia, and the Loess Plateau, where the $^{129}I/^{127}I$ number ratios in surface soil fell below 60×10^{-10}, apparently much lower than those in aerosols (Zhang et al., 2011). Furthermore, the back-trajectory analysis also showed that the low ^{129}I level on April 18 can be partially attributed to an ^{129}I-poor low-altitude air mass (< 900m) (Fig. S3a). This is because either the low-altitude air mass might be formed in ^{129}I-poor inland areas, not from the ^{129}I-rich European area, or long-range transported ^{129}I in low-altitude air mass could be easily lost by the topographic countercheck (Dong et al., 2018).

The second dust storm has started from the south-central Mongolia and the west-central Inner Mongolia autonomous region since 3 May, arrived at Xi'an on 5 May and retreated on 6 May. It is pity that no sample was analysed in this event, but a significant ^{129}I peak with value of 7.53×10^{5} atoms m^{-3} was found after three days of this event (Fig. 2b). The back-trajectory analysis suggests the ^{129}I peak on May 8, 2017 is found to relate to the downdraft originated from high altitude (2000-6000 m) to low altitude (500 m) (Fig. S3b). This elevation of ^{129}I after the dust storm events is likely attributed that the intensified winter monsoon and strong cold high pressure transporting greater ^{129}I from Europe to China.

4.2.2 Heavy haze episodes during 2017/2018 winter

A significantly positive correlation between ^{127}I and air quality index (AQI) was found with a high Spearman correlation coefficient of 0.72 ($p<<0.05$) for the whole-year sampling period, and an increased coefficient of 0.87 in winter (Table 1). The ^{127}I concentration in winter can reach up to 10 times as much as in summer (Fig. 2a). Furthermore, five ^{127}I peaks from 12.8 to 21.4 ng m^{-3} were clearly identified on 15 and 29 November, 14 and 28 December, and 16 January, respectively, which well coincided with the heavy haze episodes with AQI mostly over 200, namely heavily polluted air (Fig. 2e). As discussed in section 4.1, the irrelevance between ^{127}I and ^{129}I in aerosols for each season attributed to their different sources, also demonstrates that locally discharged iodine and externally input iodine are not contemporaneously subjected to formation of iodine-containing particles.

Further analysis showed close relationship between ^{127}I and six air pollutants, including PM 10, PM 2.5, CO, SO_2, NO_2 and O_3 (Table 1 and Fig. S4). In spring and summer, the high correlation between ^{127}I and AQI can be attributed to the high correlation between ^{127}I with PM10 and PM2.5. In fall and winter, ^{127}I, is significantly positively correlated with PM 10, PM 2.5, CO, SO_2 and NO_2, and negatively correlated with O_3. In contrast, there is no such good agreement between ^{129}I and these gaseous pollutants. Despite that, three ^{129}I peaks were found on 15 November, 14 December, 2017 and 16 January 2018, respectively, which well corresponded with high ^{127}I concentrations (Fig. 2a and 2b) during the haze episodes. This reflects that the formation mechanism of iodine-containing aerosols might be seasonally different. However, the three peaks of ^{129}I in

aerosols during the heavy haze episodes suggest that local and external iodine are likely subjected to subsequent growth of particles and capture by particles due to a longer residence time in stagnant weather conditions.

Table 1. Spearman correlation coefficients between iodine isotopes and atmospheric pollutants and weather conditions *

Correlation	Whole year				Spring (3-5)				Summer (6-8)				Fall (9-11)				Winter (12-2)			
	^{127}I		^{129}I		^{127}I		^{129}I		^{127}I		129I		^{127}I		^{129}I		^{127}I		^{129}I	
	Spear.	Sig.	Spear.	Sig.	Spear.	Sig.	Spear.	Sig.	Spear.	Sig.	Spear.	Sig.	Spear.	Sig.	Spear.	Sig.	Spear.	Sig.	Spear.	Sig.
^{129}I	**0.33**	**0.01**			-0.05	0.86			0.35	0.17			0.04	0.86			0.51	0.08		
$^{129}I/^{127}I$	**-0.28**	**0.02**	**0.74**	**0.00**	**-0.64**	**0.01**	**0.77**	**0.00**	-0.03	0.90	**0.87**	**0.00**	**-0.65**	**0.00**	**0.60**	**0.00**	**-0.94**	**0.00**	-0.35	0.25
Temp	**-0.53**	**0.00**	**-0.47**	**0.00**	-0.09	0.75	-0.21	0.44	-0.15	0.55	-0.37	0.14	**-0.54**	**0.01**	0.07	0.75	0.13	0.67	-0.19	0.53
Humidity	-0.06	0.64	-0.13	0.27	0.24	0.37	**-0.53**	**0.04**	-0.06	0.82	0.29	0.26	**-0.45**	**0.04**	-0.30	0.18	**0.69**	**0.01**	0.34	0.26
Wind speed	-0.19	0.13	-0.21	0.09	-0.08	0.76	-0.31	0.24	-0.09	0.73	0.02	0.95	0.05	0.81	0.14	0.54	-0.34	0.26	0.14	0.65
Precipitation	-0.14	0.25	-0.18	0.15	-0.04	0.88	-0.13	0.64	0.04	0.87	0.42	0.09	-0.29	0.19	-0.39	0.07	0.15	0.61	0.00	1.00
AQI	**0.72**	**0.00**	0.17	0.17	**0.95**	**0.00**	-0.05	0.85	**0.59**	**0.01**	-0.01	0.97	**0.56**	**0.01**	0.13	0.55	**0.87**	**0.00**	0.45	0.12
CO	**0.54**	**0.00**	0.20	0.11	**0.66**	**0.01**	0.19	0.49	0.17	0.52	**0.56**	**0.02**	**0.46**	**0.03**	-0.18	0.42	**0.85**	**0.00**	0.40	0.18
SO_2	**0.60**	**0.00**	**0.47**	**0.00**	0.24	0.38	-0.14	0.59	0.37	0.15	0.22	0.40	**0.53**	**0.01**	0.26	0.25	0.48	0.10	0.26	0.38
NO_2	**0.63**	**0.00**	**0.42**	**0.00**	0.45	0.08	0.00	0.99	0.13	0.61	0.27	0.30	**0.61**	**0.00**	0.08	0.74	**0.73**	**0.00**	0.14	0.64
O_3	**-0.44**	**0.00**	**-0.33**	**0.01**	-0.32	0.23	0.09	0.75	0.39	0.12	-0.37	0.15	-0.20	0.37	0.28	0.21	**-0.64**	**0.02**	-0.11	0.72
PM10	**0.71**	**0.00**	**0.24**	**0.05**	**0.84**	**0.00**	0.00	0.99	**0.74**	**0.00**	0.21	0.42	**0.51**	**0.02**	0.14	0.54	**0.84**	**0.00**	0.50	0.08
PM2.5	**0.75**	**0.00**	**0.24**	**0.05**	**0.94**	**0.00**	0.00	1.00	**0.76**	**0.00**	0.19	0.47	**0.45**	**0.03**	0.10	0.67	**0.85**	**0.00**	0.47	0.11

* Spearman correlation coefficient is used. 2-tailed test of significance is used. Correlation significant at the 0.05 level is in bold.

4.2.3 Impact of EAM for long-range transport of ^{129}I

Increasing evidence have suggested that the prevailing westerly and EAM system act as crucial driving forces and pathways for transport of the European NFRPs derived ^{129}I from Europe to East Asia and even to low-latitude southeast Asia (Fan et al., 2016; Zhang et al., 2018a). Monthly variations of atmospheric ^{129}I in Japan also showed a clear pattern with low ^{129}I deposition in summer and high in winter, which is also attributed to the impact of EAM (Hasegawa et al., 2017; Kadowaki et al., 2018; Toyama et al., 2013). In this work, seasonal variation of ^{129}I was identical to the observation in the previous studies (Toyama et al., 2013). However, the day-resolution variation patterns of ^{129}I and $^{129}I/^{127}I$ in Xi'an, distinct from monthly variation in Japan, showed three periods with high levels and two periods with low levels, indicating more complex influence of EAM in the typically continental monsoon climate city, Xi'an.

The whole-year time series can be divided into five periods with three high-level periods (HLP), a) from late March to early May (HLP 1), b) from middle August to early September (HLP 2), and c) from middle November, 2017 to late February, 2018 (HLP 3); as well as two low-level periods (LLP), d) from early May to middle August (LLP 1), and e) from middle September to early November, 2017 (LLP 2) (Fig. 2b and 2c). ^{129}I levels in the three HLPs fell within the range of (1.98-2.41) $\times 10^5$ atoms m^{-3}, which is 3-5 times higher than those during the two LLPs with (0.49-0.66) $\times 10^5$ atoms m^{-3} (Table S1). The relative standard deviation shows much higher variability during HLP 1 and 2 from 91% to 109% in contrast to the variability in other clusters less than 60%.

The significant difference between the HLPs and LLPs suggests the transportation process of ^{129}I is obviously distinct. The westerly is a crucial driving force of ^{129}I from the NFRPs point sources and their contaminated seas, and labelled by a high ^{129}I level up to 10^{-6} for $^{129}I/^{127}I$ number ratio (Michel et al., 2012; Zhang et al., 2016) (Fig. 1a). Due to interplay between westerly

and EAWM (An et al., 2012), EAWM inherits the high ^{129}I feature of 10^{-7}-10^{-9} for $^{129}I/^{127}I$ number ratio in the long-distance transport process. Therefore, the HLP 1 and 3 was strongly affected by the EAWM prevailing from early September to early may in 2017. Compared to the violent fluctuation of ^{129}I in spring (HLP1), the weak fluctuations of HLP 3 in winter might be attributed to a relatively stable interaction process between the strengthened westerly and the EAWM. In addition, the ^{129}I level in March 2018 was much less than that in March 2017, seems to be consequences of weaker EAWM strength in March 2018 compared to in March 2017. This is in good agreement with the EAWM index of 2.04 in 2017 and -1.86 in 2018 (MODES forecast motor (NCEP I), 2019). The HLP 2 was not the case as HLPs 1 and 3, since the period should be under control of EASM.

The EASM origins from the Pacific and Indian tropical under the role of subtropical highs, and transports moisture from the ocean to East Asia since early summer. $^{129}I/^{127}I$ number ratios in the Pacific Ocean, the East China Seas, and the Indian Ocean are as low as 10^{-10} (Liu et al., 2016; Povinec et al., 2011). Even after the Fukushima accident, $^{129}I/^{127}I$ number ratios are still less than 40×10^{-10} in the western Pacific Ocean (Guilderson et al., 2014). Thus, EASM is poor in ^{129}I in comparison to the winter monsoon. This is well in agreement with the low ^{129}I level during the two LLPs (Fig. 2b). The 850 hPa water vapor transmission flow field showed that the southeast wind moisture moving northward to the north of 35°N May 2, followed by another two outbreaks of on May 21 and June 3 (Fig. S5), indicative of EAWM retreat and EASM advance. During this period, ^{129}I dropped abruptly from 3.45×10^5 atoms m^{-3} on 27th April to 1.10×10^5 atoms m^{-3} on 2nd May, followed by a maximum on 8th May, then have a sudden decline to 0.64×10^5 atoms m^{-3} on 15th May. The violet fluctuation of ^{129}I is likely caused by the onset of EASM, which is quite violent in a way of stepwise northward jumps. This conclusion is fully supported by the previous metrological observations (Ding and Chan, 2005). As the EASM turned into the active stage since mid-May, ^{129}I level was low and in a relatively stable state, as showed in the LLP 1.

After the active stage of EASM, however, it is out of the expectation that increased and variable ^{129}I levels were observed from middle August to early September (HLP 2). The ^{129}I peak on September 6, 2017 was the highest throughout the sampling year. The back-trajectory model shows that five low-altitude air masses (< 1000 m above ground level) from the Baltic Sea moved fast eastward and arrived at the Guanzhong Basin within five days (Fig. S3e). The Baltic Sea contains high ^{129}I concentration due to the water exchange with the North Sea that receives over 100 kg $year^{-1}$ ^{129}I from La Hague and Sellafield NFRPs (Snyder et al., 2010). Therefore, a ^{129}I peak observed here indicates the ^{129}I-enriched westerly has interplayed with the EASM, the latter of which was retreating to the south. It is reported that Xi'an enters into the EASM break stage during this time based on the rainfall data (Ding and Chan, 2005). The intensive interaction between westerly and EASM facilitates the formation of rainfall at their confluence area, resulting in the drastically fluctuating ^{129}I levels. Therefore, the elevated and variable ^{129}I levels in HLP 2 can be attributed to the EASM break stage.

After the break stage with significant ^{129}I fluctuation, the second LLP of ^{129}I from 21st September to 11th October (LLP 2) occurred when the summer monsoon turns into the revival stage (Fig. 2b). Despite lower than the break period, the ^{129}I level in this period has slightly increased from 0.49×10^5 atoms m^{-3} in the active stage to 0.66×10^5 atoms m^{-3} in the revival stage. After the active-break-revival cycle of summer monsoon reflected by low-high-low ^{129}I level, the ^{129}I level has stepwise

increased since mid-October, suggesting the EAWM has taken the place of the EASM in the Guanzhong Basin, and last until March next year.

To quantitatively characterize the influence of EAM on variation of ^{129}I, z-normalized ^{129}I concentrations and $^{129}I/^{127}I$ number ratios were used to build a quantitative model during winter monsoon and different stages of the summer monsoon including onset, active, break, revival and retreat (Fig. 6). Z(^{129}I) varies from -1.11 to 3.38 with a median value of -0.29, and z($^{129}I/^{127}I$ number ratio) from -0.66 to 5.26 with a median value of -0.34. Based on the observation during 2017/2018 in the Guanzhong Basin, when z(^{129}I) is less than -0.5 and z($^{129}I/^{127}I$ number ratio) is smaller than 0, this period is in good agreement with the onset, active and revival stages of the EASM. During the stable active-stage, z-scores for ^{129}I and $^{129}I/^{127}I$ were minimal, which was followed by the second lowest value during the revival stage. The onset and break stage showed much larger fluctuation with z-scores changing from -0.8 to -0.3. The break stage of East Asia summer monsoon is an exception, which exists alternative influence from both factors in our studied region. The z(^{129}I) from 1.57 to 1.96 of the break stages were even much higher than the period controlled by East Asia winter monsoon with z(^{129}I) from -0.5 to 1.53. This result clearly confirms that the EAM plays a decisive role on the temporal variation and long-range transport of not only ^{129}I, but also other air pollutants (i.e. persisting organic pollutants, inorganic air pollutants) in Chinese monsoon-affected regions.

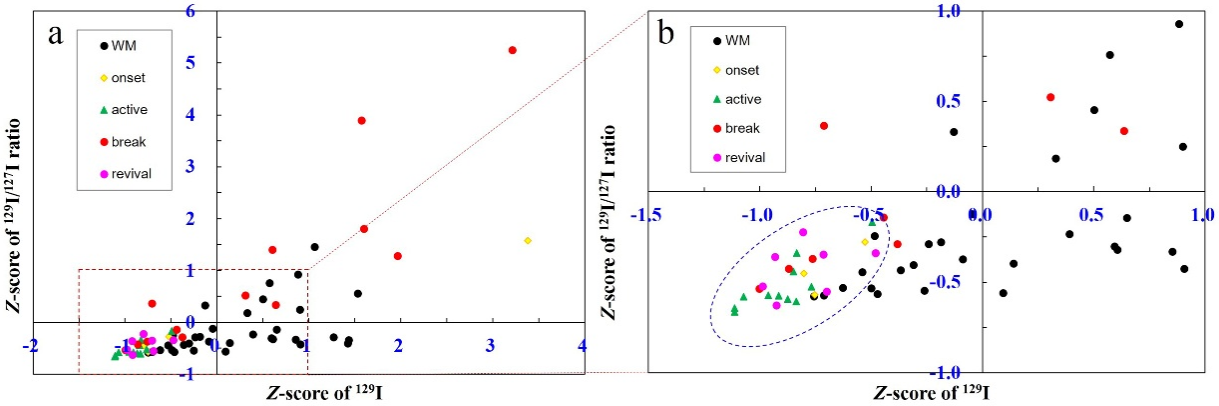

Fig. 6 Two-dimension graph of z-score normalized ^{129}I concentrations and $^{129}I/^{127}I$ number ratios, suggesting the refined features of East Asia summer (onset, active, break and revival in yellow diamond, green triangle, red circle and pink circle, respectively) and winter monsoons (WM, black dot) (a). The coloured symbols clearly demonstrate a detailed cycle of onset-active-break-revival for the summer monsoon with $Z_{129I} \leq -0.5$ and $Z_{Ratio} \leq 0$, as illustrated in the blue oval area (b).

4.3 Atmospheric background level of $^{129}I/^{127}I$ number ratio

For the purpose of nuclear environment safety monitoring, the average $^{129}I/^{127}I$ number ratio of $(92.7 \pm 124) \times 10^{-10}$ can be simply regarded as the atmospheric background level of ^{129}I in northwest China. The previous studies on ^{129}I environmental baseline have never carefully investigate the influence of weather on time variation of ^{129}I. Here our day-resolution ^{129}I dataset in this monsoon climate city showed that time variation of the atmospheric baseline level related to metrological conditions, heavy haze events and atmospheric circulation, has to be carefully considered and used for better evaluation of the impact of possible

nuclear incidents in a practical way. Particularly, a pilot nuclear reprocessing plants locating upwind to Xi'an, might be extended and will be a source of radionuclides in the future. The baseline established in this work is, therefore, of significance to long-term monitor nuclear environmental safety, and to sensitively assess the impact of nuclear incidents and apply on environmental process tracing.

5 Conclusions

The study firstly presents a high-resolution temporal variation of atmospheric ^{127}I and ^{129}I in northwest China, showing the vivid seasonal characteristics of iodine isotopes and an $^{129}I/^{127}I$ baseline ratio of (92.7±124) $\times 10^{-10}$. Variation of ^{127}I strongly linking with atmospheric pollutions and heavy haze episodes, in particular in winter, indicates that ^{127}I in Xi'an aerosols mainly derives from combustion of fossil fuel. Aerosol ^{129}I mainly originates from European nuclear reprocessing plants through long-range transport, and its temporal variation is strongly dominated by the interplay of East Asian winter and summer monsoon. Previous studies on temporal changes of atmospheric ^{129}I in other monsoonal regions showed a simple pattern with lowest level in summer and highest in winter, while our day-resolution dataset showed that high ^{129}I levels could be found in summer time due to the break of East Asian summer monsoon. The locally input ^{127}I and exogenous ^{129}I were greatly increased during haze events, reflecting the possible role of iodine in the formation of urban fine particles, therefore, further investigations are expected to focus on the speciation of iodine isotopes for mechanism study of iodine's impact on air pollution.

Supplement

Supplementary information accompanies this paper in a separate file.

Author contribution

LZ, XH and SX designed and optimized the experiment. LZ, and NC performed the experiment, with the help of PC and YF. TF collected the air pollutant data. LZ, TF, PC, and YF draw the figures. The data analysis and interpretation were carried out by LZ, XH, SX, TF and NC. LZ prepared the paper, with contributions from all co-authors.

Competing interests

The authors declare that they have no conflict of interests.

Acknowledgement

This work was supported by the National Natural Science Foundation of China (No. 11605207 and 41603125), the Youth Innovation Promotion Association of CAS, the Ministry of Science and Technology basic project (No. 2015FY110800), the Bureau of International Co-operation, CAS (132B61KYSB20180003) and National Research Program for Key Issues in Air

Pollution Control (DQGG0105). L.Z. also gratefully acknowledges Dr. Q. Liu, Ms. M. Fang, Ms. Y. Wang, Mr. L. Wang and Mr. J. Zhou in IEECAS for their kind helps on AMS measurement, sample collection and figure drawing. We acknowledge the two anonymous referees for their constructive comments.

References

An, Z., Colman, S. M., Zhou, W., Li, X., Brown, E. T., Jull, A. J. T., Cai, Y., Huang, Y., Lu, X., Chang, H., Song, Y., Sun, Y., Xu, H., Liu, W., Jin, Z., Liu, X., Cheng, P., Liu, Y., Ai, L., Li, X., Liu, X., Yan, L., Shi, Z., Wang, X., Wu, F., Qiang, X., Dong, J., Lu, F. and Xu, X.: Interplay between the Westerlies and Asian monsoon recorded in Lake Qinghai sediments since 32 ka, Sci. Rep., 2, 619, doi.org/10.1038/srep00619, 2012.

Ayers, G. P., Penkett, S. A., Gillett, R. W., Bandy, B., Galbally, I. E., Meyer, C. P., Elsworth, C. M., Bentley, S. T. and Forgan, B. W.: The annual cycle of peroxides and ozone in marine air at Cape Grim, Tasmania, J. Atmos. Chem., 23(3), 221–252, doi:10.1007/BF00055155, 1996.

Brauer, F. P., Rieck, H. G. J. and Hooper, R. L.: Particulate and gaseous atmospheric iodine concentrations, IAEA, International Atomic Energy Agency (IAEA)., 1973.

Carpenter, L. J., MacDonald, S. M., Shaw, M. D., Kumar, R., Saunders, R. W., Parthipan, R., Wilson, J. and Plane, J. M. C.: Atmospheric iodine levels influenced by sea surface emissions of inorganic iodine, Nat. Geosci., 6(2), 108–111, doi:10.1038/ngeo1687, 2013.

Cheng, N., Duan, L., Xiu, G., Zhao, M. and Qian, G.: Comparison of atmospheric PM2.5-bounded mercury species and their correlation with bromine and iodine at coastal urban and island sites in the eastern China, Atmos. Res., 183, 17–25, doi:10.1016/j.atmosres.2016.08.009, 2017.

China Meteororological Administration: Sandstorm in northwest China and central and western Inner Mongolia, Webpage [online] Available from: http://www.cma.gov.cn/2011xwzx/2011xqxxw/2011xzytq/201704/t20170417_407699.html (Accessed 10 October 2018), 2017.

Cohen, B. L.: The origin of I in soil and the ^{129}I problem, Health Phys., 49(2), 279–285, 1985.

Ding, Y. and Chan, J. C. L.: The East Asian summer monsoon: An overview, Meteorol. Atmos. Phys., 89(1–4), 117–142, doi:10.1007/s00703-005-0125-z, 2005.

Dong, Z., Shao, Y., Qin, D., Zhang, L., Hou, X., Wei, T., Kang, S. and Qin, X.: Insight Into Radio-Isotope ^{129}I Deposition in Fresh Snow at a Remote Glacier Basin of Northeast Tibetan Plateau, China, Geophys. Res. Lett., 0(0), doi:10.1029/2018GL078480, 2018.

Duan, D.: Concentration Characteristics of Atmospheric Particulate Matters and Iodine in Coal-fired Area, Nanchang University., 2018.

Englund, E., Aldahan, A., Hou, X., Possnert, G. and Soderstrom, C.: Iodine (I-129 and I-127) in aerosols from northern Europe, Nucl.Instrum.Meth.B, 268(7–8), 1139–1141, 2010.

Fan, Y.: Spatial distribution of ^{129}I in Chinese surface soil and preliminary study on the ^{129}I chronology, PhD thesis. Inst. Earth Environ. Chinese Acad. Sci., 2013.

Fan, Y., Hou, X., Zhou, W. and Liu, G.: I record of nuclear activities in marine sediment core from Jiaozhou Bay in China, J. Environ. Radioact., 154(March 2011), 15–24, doi:10.1016/j.jenvrad.2016.01.008, 2016.

Fehn, U., Moran, J. E., Snyder, G. T. and Muramatsu, Y.: The initial ^{129}I/I ratio and the presence of "old" iodine in continental margins, Nucl.Instrum.Meth.B, 259(1), 496–502, 2005.

Fuge, R. and Johnson, C.: The geochemistry of iodine - a review, Environ. Geochem. Health, 8(2), 31–54, doi:10.1007/BF02311063, 1986.

Gao, Y., Sun, M., Wu, X., Liu, Y., Guo, Y. and Wu, J.: Concentration characteristics of bromine and iodine in aerosols in Shanghai, China, Atmos. Environ., 44, 4298–4302, doi:10.1016/j.atmosenv.2010.05.047, 2010.

Guilderson, T. P., Tumey, S. J., Brown, T. a. and Buesseler, K. O.: The 129-iodine content of subtropical Pacific waters: impact of Fukushima and other anthropogenic ^{129}I sources, Biogeosciences, 11, 4839–4852, doi:10.5194/bgd-10-19935-2013, 2014.

Hasegawa, H., Kakiuchi, H., Akata, N., Ohtsuka, Y. and Hisamatsu, S.: Regional and global contributions of anthropogenic iodine-129 in monthly deposition samples collected in North East Japan between 2006 and 2015, J. Environ. Radioact., 171, 65–73, doi:10.1016/J.JENVRAD.2017.01.027, 2017.

He, C., Hou, X., Zhao, Y., Wang, Z., Li, H., Chen, N., Liu, Q., Zhang, L., Luo, M., Liang, W., Fan, Y. and Zhao, X. L.: ^{129}I level in seawater near a nuclear power plant determined by accelerator mass spectrometer, Nucl. Instruments Methods Phys. Res. Sect. A, 632(1), 152–156, doi:10.1016/j.nima.2010.12.182, 2011.

He, L.: Iodine concentration, chemical speciation and their distribution in atmospheric precipitation and soil, Nanchang University, China., 2012.

Hou, X., Aldahan, A., Nielsen, S. P., Possnert, G., Hou, X., Aldahan, A., Nielsen, S. P. and Possnert, G.: Time Series of I-129 and I-127 Speciation in Precipitation from Denmark, Environ. Sci. Technol., 43(17), 6522–6528, doi:10.1021/es9012678, 2009.

Jabbar, T., Wallner, G. and Steier, P.: A review on ^{129}I analysis in air, J. Environ. Radioact., 126, 45–54, 2013.

Jackson, D., Ibrahimi, F., Fulker, M. J., Parry, S. J. and Rackham, K.: The effect of chemical speciation on the impact of I discharges to atmosphere from BNFL Sellafield, Cumbria, Radioprotection, 37(C1), 459–464, 2002.

Kadowaki, M., Katata, G., Terada, H., Suzuki, T., Hasegawa, H., Akata, N. and Kakiuchi, H.: Impacts of anthropogenic source from the nuclear fuel reprocessing plants on global atmospheric iodine-129 cycle: A model analysis, Atmos. Environ., 184(April), 278–291, doi:10.1016/j.atmosenv.2018.04.044, 2018.

Küpper, F. C., Carpenter, L. J., McFiggans, G. B., Palmer, C. J., Waite, T. J., Boneberg, E.-M., Woitsch, S., Weiller, M., Abela, R., Grolimund, D., Potin, P., Butler, A., Luther, G. W. 3rd, Kroneck, P. M. H., Meyer-Klaucke, W. and Feiters, M. C.: Iodide accumulation provides kelp with an inorganic antioxidant impacting atmospheric chemistry, Proc. Natl. Acad. Sci., 105(19), 6954–6958, 2008.

Liu, D., Hou, X., Du, J., Zhang, L. and Zhou, W.: ^{129}I and its species in the East China Sea: level, distribution, sources and tracing water masses exchange and movement, Sci. Rep., 6(October), 36611, doi:10.1038/srep36611, 2016.

McFiggans, G., Plane, J. M. C., Allan, B. J., Carpenter, L. J., Coe, H. and O'Dowd, C.: A modeling study of iodine chemistry in the marine boundary layer, J. Geophys. Res. Atmos., 105(D11), 14371–14385, doi:10.1029/1999JD901187, 2000.

Michel, R., Daraoui, A., Gorny, M., Jakob, D., Sachse, R., Tosch, L., Nies, H., Goroncy, I., Herrmann, J., Synal, H. A., Stocker, M. and Alfimov, V.: Iodine-129 and iodine-127 in European seawaters and in precipitation from Northern Germany, Sci.Total Environ., 419, 151–169, 2012.

Ministry of Environmental Protection of the People's Republic of China: Environmental radiation monitoring results of the sixth North Korean nuclear test in the northeast border and surrounding areas., 2017.

MODES forecast motor (NCEP I): East Asian Winter Monsoon Index, Beijing Clim. Cent. [online] Available from: https://cmdp.ncc-cma.net/pred/cn_peace.php?eYear=2017&eMonth=5&search=¢%D0%CE¸&product=EAWM.MODES#search (Accessed 8 July 2019), 2019.

Moran, J. E., Oktay, S. D., Santschi, P. H. and Schink, D. R.: Atmospheric dispersal of iodine-129 from nuclear fuel reprocessing facilities, Environ. Sci. Technol., 33(15), 2536–2542, 1999.

Povinec, P. P., Breier, R., Coppola, L., Groening, M., Jeandel, C., Jull, A. J. T., Kieser, W. E., Lee, S. H., Liong, W. K., Morgenstern, U., Park, Y. H. and Top, Z.: Tracing of water masses using a multi isotope approach in the southern Indian Ocean, Earth Planet. Sci. Lett., 302(1–2), 14–26, 2011.

Saiz-Lopez, A., Gómez Martín, J. C., Plane, J. M. C., Saunders, R. W., Baker, A. R., Von Glasow, R., Carpenter, L. J. and McFiggans, G.: Atmospheric chemistry of iodine, Chem. Rev., 112(3), 1773–1804, 2012.

Santos, F. J., López-Gutiérrez, J. M., García-León, M., Suter, M. and Synal, H. A.: Determination of ^{129}I/^{127}I in aerosol samples in Seville (Spain), J. Environ. Radioact., 84(1), 103–109, 2005.

Shaanxi Provincial Bureau of Statistics: Report of industrial coal reduction in Guanzhong Basin in 2017, Xi'an, China. [online] Available from: http://www.shaanxitj.gov.cn/site/1/html/126/131/138/17703.htm, 2018.

Sive, B. C., Varner, R. K., Mao, H., Talbot, R., Blake, D. R. and Wingenter, O. W.: A large terrestrial source of methyl iodide, Geophys. Res. Lett., 34(17), 2007.

Snyder, G., Aldahan, A., Aldahan, A. and Possnert, G.: Global distribution and long-term fate of anthropogenic ^{129}I in marine and surface water reservoirs, Geochemistry, Geophys. Geosystems, 11(4), 1–19, 2010.

Toyama, C., Muramatsu, Y., Igarashi, Y., Aoyama, M. and Matsuzaki, H.: Atmospheric fallout of ^{129}I in Japan before the Fukushima accident: Regional and global contributions (1963-2005), Environ. Sci. Technol., 47(15), 8383–8390, doi:10.1021/es401596z, 2013.

Tsukada, H., Ishida, J. and Narita, O.: Particle-size distributions of atmospheric ^{129}I and ^{127}I aerosols, Atmos. Environ. Part A, 25(5–6), 905–908, doi:http://dx.doi.org/10.1016/0960-1686(91)90132-Q, 1991.

Wershofen, H. and Aumann, D. C.: Iodine-129 in the environment of a nuclear fuel reprocessing plant: VII. Concentrations

and chemical forms of ^{129}I and ^{127}I in the atmosphere, J. Environ. Radioact., 10(2), 141–156, 1989.

Whitehead, D. C.: The distribution and transformations of iodine in the environment, Environ. Int., 10(4), 321–339, doi:10.1016/0160-4120(84)90139-9, 1984.

World Nuclear Association: http://www.world-nuclear.org/, Last access 9 Jan 2017, 2017.

Wu, D., Du, J., Deng, H., Wang, W., Xiao, H. and Li, P.: Estimation of atmospheric iodine emission from coal combustion, Int. J. Environ. Sci. Technol., 11(2), 357–366, doi:10.1007/s13762-013-0193-4, 2014.

Xi'an Bureau of Statistics: Xi'an Statistics Yearbook. [online] Available from: http://tjj.xa.gov.cn/ptl/def/def/2017/zk/indexch.htm, 2018.

Xu, S., Xie, Z., Li, B., Liu, W., Sun, L., Kang, H., Yang, H. and Zhang, P.: Iodine speciation in marine aerosols along a 15000-km round-trip cruise path from Shanghai, China, to the Arctic Ocean, Environ. Chem., 7(5), 406–412 [online] Available from: http://dx.doi.org/10.1071/EN10048, 2010.

Xu, S., Freeman, S. P. H. T. S. P. H. T., Hou, X., Watanabe, A., Yamaguchi, K. and Zhang, L.: Iodine Isotopes in Precipitation: Temporal Responses to ^{129}I Emissions from the Fukushima Nuclear Accident, Environ. Sci. Technol., 47(19), 10851–10859, doi:10.1021/es401527q, 2013.

Xu, S., Zhang, L., Freeman, S. P. H. T., Hou, X., Shibata, Y., Sanderson, D., Cresswell, A., Doi, T. and Tanaka, A.: Speciation of Radiocesium and Radioiodine in Aerosols from Tsukuba after the Fukushima Nuclear Accident, Environ. Sci. Technol., 49(2), 1017–1024, doi:10.1021/es504431w, 2015.

Zhang, L., Zhou, W. J., Hou, X., Chen, N., Liu, Q., He, C., Fan, Y., Luo, M., Wang, Z. and Fu, Y.: Level and source of ^{129}I of environmental samples in Xi'an region, China, Sci. Total Environ., 409(19), 3780–3788, doi:10.1016/j.scitotenv.2011.06.007, 2011a.

Zhang, L., Hou, X. and Xu, S.: Speciation of ^{127}I and ^{129}I in atmospheric aerosols at Risø, Denmark: Insight into sources of iodine isotopes and their species transformations, Atmos. Chem. Phys., 16, 1971–1985, 2016.

Zhang, L., Hou, X., Li, H. and Xu, X.: A 60-year record of ^{129}I in Taal Lake sediments (Philippines): Influence of human nuclear activities at low latitude region, Chemosphere, 193, 1149–1156, doi:10.1016/j.chemosphere.2017.11.134, 2018a.

Zhang, L., Hou, X., Fu, Y., Fang, M. and Chen, N.: Determination of ^{129}I in aerosols using pyrolysis and AgI–AgCl coprecipitation separation and accelerator mass spectrometry measurements, J. Anal. At. Spectrom., 33, 1729–1736, doi:10.1039/C8JA00248G, 2018b.